Available online at www.sciencedirect.com

SCIENCE DIRECT

Remote Sensing of Environment 94 (2005) 46–60

Remote Sensing of Environment

www.elsevier.com/locate/rse

Accuracy assessment of the MODIS 16-day albedo product for snow: comparisons with Greenland in situ measurements

Julienne Stroeve*, Jason E. Box, Feng Gao, Shunlin Liang, Anne Nolin, Crystal Schaaf

National Snow and Ice Data Center (NSIDC), University of Colorado, Campus Box 449, Boulder, CO 80309-0449, United States

Received 18 May 2004; received in revised form 2 September 2004; accepted 6 September 2004

Abstract

The accuracy of the Moderate Resolution Imaging Spectroradiometer (MODIS) 16-day albedo product (MOD43) is assessed using ground-based albedo observations from automatic weather stations (AWS) over spatially homogeneous snow and semihomogeneous ice-covered surfaces on the Greenland ice sheet. Data from 16 AWS locations, spanning the years 2000–2003, were used for this assessment. In situ reflected shortwave data were corrected for a systematic positive spectral sensitivity bias of between 0.01 and 0.09 on a site-by-site basis using precise optical black radiometer data. Results indicate that the MOD43 albedo product retrieves snow albedo with an average root mean square error (RMSE) of ± 0.07 as compared to the station measurements, which have ± 0.035 RMSE uncertainty. If we eliminate all satellite retrievals that rely on the backup algorithm and consider only the highest quality results from the primary bidirectional reflectance distribution function (BRDF) algorithm, the MODIS albedo RMSE is ± 0.04, slightly larger than the in situ measurement uncertainty. There is general agreement between MODIS and in situ observations for albedo <0.7, while near the upper limit, a -0.05 MODIS albedo bias is evident from the scatter of the 16-site composite.

Keywords: MODIS; Snow; Greenland

1. Introduction

Surface albedo is the ratio of upwelling radiant energy relative to the downwelling irradiance incident upon a surface. Snow and ice cover, with its high albedo, is a critical component of the global energy budget, as snow reflects the majority of incident solar radiation back to space. New snow reflects more than 80% of the incident radiation, thereby allowing very little solar energy to be absorbed. However, as snow ages and/or begins to melt, developing into firn or exposing bare ice, its albedo is greatly reduced, leading to enhanced solar radiation absorption, further reducing the albedo through amplified melting in a positive feedback loop. For instance, coarse-grained (e.g., old and/or wet) snow typically has an albedo on the order of 0.5, so absorption of shortwave radiation is a factor of 3 greater than that of fine-grained fresh snow, with an albedo of about 0.85.

Since vast expanses of the Earth's polar regions are permanently covered by snow and ice (e.g., the Greenland and Antarctic ice sheets), satellite remote sensing offers the only practical means to monitor changes in snow albedo at high spatial and temporal resolutions. Surface albedo of the polar regions has been monitored using a number of space-borne sensors. The longest and most consistent set of observations of large-scale surface albedo variations over the polar regions is available from the Advanced Very High Resolution Radiometer (AVHRR) Polar Pathfinder (APP) data set (e.g., Maslanik et al., 1998). However, AVHRR has only two narrow spectral bands in the visible/near-infrared (NIR) portion of the spectrum, limiting its accuracy and sensitivity to changes in broadband albedo. The Moderate Resolution Imaging Spectroradiometer (MODIS) is a key instrument aboard both the NASA's Terra and Aqua

* Corresponding author. Tel.: +1 303 492 3584; fax: +1 303 492 2468.
E-mail address: stroeve@kryos.colorado.edu (J. Stroeve).

0034-4257/$ - see front matter
doi:10.1016/j.rse.2004.09.001

satellites, viewing the regions poleward of 60° as many as 10–14 times a day and acquiring data in 36 spectral channels in the visible, near infrared (NIR), and thermal infrared. In comparison to the AVHRR instrument, MODIS has 19 spectral channels that span the visible and NIR spectrum. Because of the higher spectral and spatial resolution of the MODIS instrument, MODIS promises to improve our ability to more precisely monitor changes in snow albedo and to enable a better understanding of the feedback mechanisms that may amplify or dampen climate variability in the polar regions. However, MODIS albedo data require further comparison with observations to assess their true accuracy.

One of the standard MODIS products is a set of land surface albedo products (known as MOD43). This study is motivated by the need to assess MOD43 albedo accuracies over spatially homogeneous snow/ice-covered surfaces. We incorporate the newly reprocessed version 4 MOD43 products, which include revised shortwave and NIR narrow-to-broadband (NTB) conversion factors for spatially homogeneous snow pixels. To assess the revised product, we compare MOD43 surface albedo values with in situ albedo measurements from 16 automatic weather stations (AWS) located at diverse locations on the Greenland ice sheet representing the 'dry snow' and perennially melting zones (Steffen & Box, 2001). Section 2 provides a summary of the MOD43 products, and Section 3 discusses in situ measurements. In Section 4, we show the comparisons between the ground-based and satellite-based estimates of the surface albedo, and a discussion of the accuracy of the MOD43 products is summarized in Section 5.

2. MODIS albedo product

2.1. Product description

The operationally archived MODIS albedo products (MOD43B3) (Schaaf et al., 2002) include the 'best-fit' bidirectional reflectance distribution function (BRDF) model parameters associated with the first seven spectral bands of MODIS (see Table 1) and three additional broadbands (0.3–0.7, 0.7–5.0, and 0.3–5.0 μm). The BRDF specifies the angular distribution of surface scattering as functions of illumination and viewing geometries at a particular wavelength. The downwelling radiative flux at the surface may be written as the sum of a direct component and a diffuse component. The directional hemispherical reflectance ("black-sky albedo") is defined as albedo in the absence of a diffuse component and is a function of solar zenith angle. The bihemispherical reflectance ("white-sky albedo") is defined as albedo in the absence of a direct component when the diffuse component is isotropic. The completely diffuse bihemispherical albedo for isotropic illumination can be derived through integration of the BRDF for the entire solar and viewing hemisphere, while the direct beam directional hemispherical albedo can be calculated through integration of the BRDF for particular illumination geometry (Martonchik et al., 2001). Actual albedo under given atmospheric and illumination conditions can be estimated as a combination of black-sky and white-sky albedos, based on the relative proportions of beam and diffuse illumination. In this paper, we use the terms WSA (white-sky albedo) and BSA (black-sky albedo) in order to maintain consistency with the terms used by the MODIS team members.

Table 1
MODIS channels used in this study

Channel	Spectral interval (nm)
1	620–670
2	841–876
3	459–479
4	545–565
5	1230–1250
6	1628–1652
7	2105–2155

In addition to the BRDF model measures, white-sky and black-sky albedos are computed for local solar noon and provided as a standard product for the same seven MODIS channel spectral bands and the three broadband regions. A third standard product, the nadir BRDF-adjusted reflectance (NBAR), for the seven spectral bands at the solar zenith angle of the mean overpass time (MOD43B4) is also archived every 16 days. These NBAR products are used as the primary input for the MODIS Land Cover and Land Cover Dynamics Products due to their stability and temporal consistency (Friedl et al., 2002). As well as the standard 1-km tiled products, these same BRDF, albedo, and NBAR data sets are also routinely produced at a 0.05° spatial resolution in a global geographic (latitude/longitude) projection specifically for use by global and regional modelers. Globally, there are 460 tiles and each tile has fixed Earth locations covering an area of approximately 1200×1200 km (10°×10° at the equator). The Collection 3 MODIS Land tile products are defined in the equal area Integerized Sinusoidal projection (Rossow & Garder, 1984), whereas the Collection 4+ MODIS Land tile products are defined in the equal area Sinusoidal projection (Snyder, 1987).

2.2. BRDF derivation

The operational MODIS BRDF/albedo algorithm makes use of a 'kernel-driven' linear BRDF model, which relies on the weighted sum of an isotropic parameter and two functions (or kernels) of viewing and illumination geometry (Roujean et al., 1992). One kernel is derived from radiative transfer models after Ross (1981), and the other is based on surface scattering and geometric shadow casting theory (Li & Strahler, 1992). All cloud-cleared, atmospherically corrected surface reflectances over a 16-day period are considered. The data are binned separately as snow-free or snow-covered. After determining whether the majority of the clear observations available represents a snow-covered or snow-free situation, the kernel weights that best fit the majority situation are selected (Lucht et al., 2000; Schaaf et al., 2002). The Ross (thick) and Li (sparse) model combination is well suited for describing surface anisotropy of global land covers (Privette et al., 1997; Lucht et al., 2000) and is similar to schemes used to obtain BRDF and albedo information by the Polarization and Directionality of Earth Reflectance (POLDER) (Bicheron & Leroy, 2000; Leroy & Hautecoeur, 1999) and Meteosat Second Generation (MSG) (Van Leeuwen & Roujean, 2002) satellite sensors.

Both the root mean square error (RMSE) of the model fit and the weights of determination (Lucht & Lewis, 2000) are assessed to determine whether these full inversions are of sufficient quality to retain and be flagged as high-quality results. Only model fits with RMSE<0.1 and weights of determination <2.5 are considered for retention as full inversions. For those locations where a full BRDF model cannot be confidently retrieved, a 'backup' algorithm is employed. This method (Strugnell & Lucht, 2001) relies on a global database of archetypal BRDF models and uses a land cover classification and a database of high-quality MODIS full inversion BRDF retrievals from a previous year. This a priori database is then used as an initial estimate of the surface BRDF and all available cloud-free observations are used to constrain the model. While, at present, as little as a single observation can be used, retrievals based on less than three observations are flagged as the absolutely lowest quality product and any retrievals using the backup algorithm are flagged as 'low-quality' results, compared to full inversion retrievals. However, it is noteworthy that while retrievals that use the backup algorithm are flagged as a lower-quality results, Jin et al. (2003a,b) have found the backup algorithm to be robust and perform quite well under most situations.

2.3. Derivation of white-sky and black-sky albedo

Once an appropriate BRDF model has been retrieved, integration over all view angles results in a directional–hemispherical black-sky albedo at any desired solar angle, and a further integration over all illumination angles results in a bihemispherical white-sky albedo. These albedo quantities are intrinsic to a specific location, are governed by the character and structure of its land cover, and can be combined with appropriate atmospheric optical depth information to produce the actual albedo for an illumination-specific geometry. The retrieved BRDF models can also be used to compute directional surface reflectances at any viewing geometry (e.g., nadir view).

Furthermore, MODIS spectral information can be incorporated via NTB conversion coefficients (Liang et al., 1999) to provide broadband BRDF models. While generalized conversion coefficients were found to work well for most land cover types, a specialized set of NTB coefficients was implemented for high albedo snow. The following NTB formula is used for derivation of the shortwave broadband albedo (α_{short}):

$$\alpha_{\mathrm{short}} = -0.0093 + 0.1574\rho_1 + 0.2789\rho_2 + 0.3829\rho_3 + 0.1131\rho_5 + 0.0694\rho_7 \quad (1)$$

where ρ is the MODIS narrowband albedo for the specified MODIS spectral channel (e.g., 1, 2, 3, 5, and 7).

A pixel is considered "pure snow" when the normalized difference vegetation index (NDVI) is less than 0.0 and the normalized difference snow index (NDSI) is larger than 0.7 (Klein & Stroeve, 2002). The NDSI is similar to the NDVI but uses the MODIS bands 4 (green spectral band) and 6 (infrared spectral band), and has high values for pixels entirely covered by snow. Therefore, together with the NDVI, it gives a conservative criterion for pure snow and application of the specialized NTB coefficients. A strict criterion for pure snow is acceptable since recent validation results show that the generalized MODIS BRDF/albedo coefficients yield accurate results for snow-covered forest regions (Jin et al., 2003b). The resulting broadband shortwave values are utilized for this study.

2.4. Other processing steps

For each ground station location discussed in Section 3, a 3×3 pixel area was extracted from the 1-km resolution MODIS Greenland tiles. However, in the Results section, we only use the center pixel to compare with the ground-based measurements. All albedo values came from 'collection 4 processing' of the MOD43B3 product and therefore utilize the most recent snow NTB coefficients given in Eq. (1). As mentioned earlier, the BRDF retrieval qualities of the primary MODIS BRDF/albedo algorithm are determined by considering the RMSE (which describes the fit of the BRDF model to the satellite measurements) and the weights of determination for both the albedo and the nadir reflectance, which shows how the angular samples are distributed in the hemisphere. If any of these retrieval quality factors are too low, the backup algorithm is used instead and the correspondingly low-quality flag then merely indicates the overall number of observations that were used with the backup algorithm. These quality flags are stored in the standard MODIS BRDF/albedo products in a separate layer. All albedo retrieval quality flags associated with the data have been extracted for the further data analysis in this study.

3. In situ snow albedo observational data

3.1. Greenland AWS

Downward and upward broadband shortwave radiation fluxes are measured at Greenland Climate Network (GC-Net) AWS distributed widely in latitude and elevation across the Greenland ice sheet (Steffen & Box, 2001) (Fig. 1 and Table 2). Shortwave fluxes are measured by pairs of LI-COR 200SZ photoelectric diode pyranometers (Table 3). The pyranometers are horizontally leveled to measure incident and reflected hemispheric radiant flux density (irradiance), and to provide hourly average shortwave albedo data from 15-s samples.

To stabilize GC-Net towers from strong winds, steel cables have been attached between the tower midsection and the snow surface at azimuth angle intervals of 120°. However, differential snow compaction has caused the towers to shift over time, leading to problems in precise radiometry. Periodic site visits have shown that most of the pyranometers were found to be acceptably level (i.e., within 1°). Data from pyranometers with leveling errors greater than 2° were not used in this assessment. To minimize the effect of leveling errors less than 1°, we produce daily average albedo data. To reduce the cosine-response error

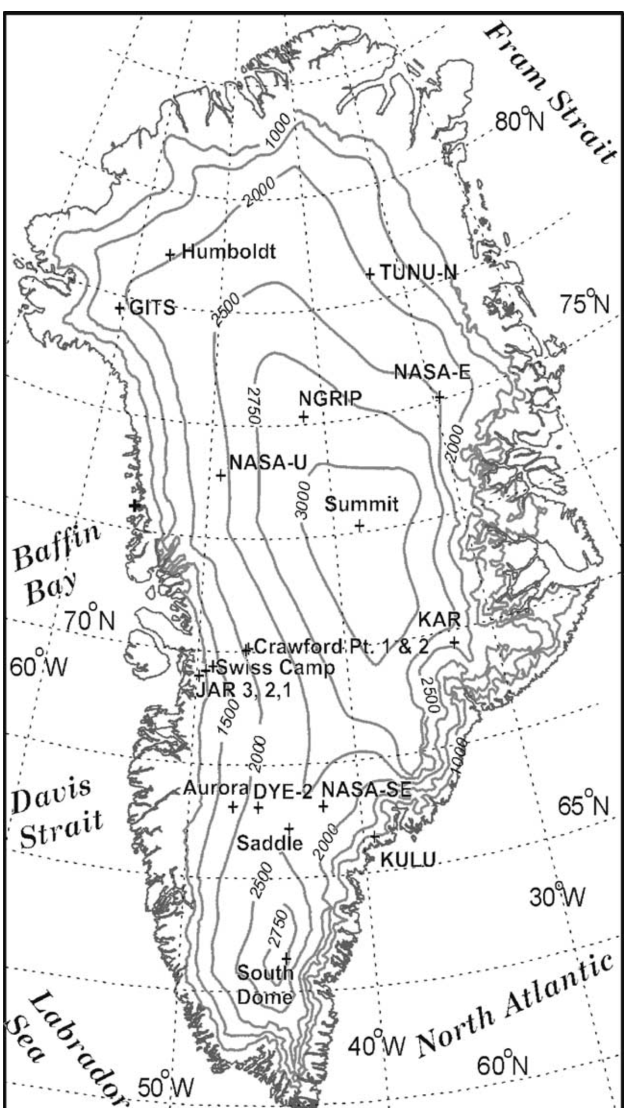

Fig. 1. Greenland map featuring the inland ice region and GC-Net locations.

Table 2
Station name and location for the Greenland AWS

Station ID number	Name	Latitude (° north)	Longitude (° west)	Elevation (m)	Start date (year/decimal day)
1	Swiss Camp	69.5732	49.2952	1149	1995.00
2	CP1	69.8819	46.9763	2022	1995.39
3	NASA-U	73.8333	49.4953	2368	1995.41
4	GITS	77.1433	69.0950	1887	1995.43
5	Humboldt	78.5266	56.8305	1995	1995.47
6	Summit	72.5794	38.5042	3208	1996.37
7	Tunu-N	78.0168	33.9939	2020	1996.38
8	DYE-2	66.4810	46.2800	2165	1996.40
9	JAR1	69.4984	49.6816	962	1996.47
10	Saddle	66.0006	44.5014	2559	1997.30
11	South Dome	63.1489	44.8167	2922	1997.31
12	NASA-E	75.0000	29.9997	2631	1997.34
13	CP2	69.9133	46.8547	1990	1997.36
14	NGRIP	75.0998	42.3326	2950	1997.52
15	NASA-SE	66.4797	42.5002	2579	1998.30
16	KAR	69.6995	32.9998	2400	1999.38
17	JAR2	69.4200	50.0575	568	1999.41
18	KULU	65.7584	39.6018	878	1999.46
19	JAR3	69.3954	50.3104	323	2000.41
20	Aurora	67.1352	47.2911	1798	2000.48

intrinsic to pyranometers, the daily mean is based on hourly values weighted by the cosine of the solar zenith angle.

The LI-COR 200SZ instrument has advantages over standard thermopile pyranometers in the ice sheet environment owing to its greater resistance to rime frost errors. The 200SZ is relatively small in size and mass, allowing the sensor body to adjust faster to temperature changes than larger radiometers. Furthermore, the detector surface is horizontal, having no dome to collect horizontally accreting frost. The limited spectral sensitivity (0.4–1.1 μm) of the LI-COR 200SZ pyranometer is a disadvantage, however, when compared to standard optical black thermopile instruments that have a nearly uniform response in the full ultraviolet to NIR (0.285–2.8 μm) range. The LI-COR instrument response is, however, factory-adjusted to account for the partial spectral sensitivity under a standard atmosphere, and gauges downward shortwave irradiance over the ice sheet within its 5% error specifications. Systematic biases occur, however, when measuring reflected irradiance over surfaces differing from a uniform gray body. In the case of snow, owing to high reflectance in the 0.3–0.7 μm wavelength range and the low reflectance for wavelengths >1.1 μm invisible to the 200SZ, the 200SZ reflected radiation data exhibit a positive bias. A correction for the positive bias was computed-based in comparison with 200SZ observations with optical black thermopile instruments.

AWS-reflected irradiance data are corrected for spectral sensitivity bias based on results from comparisons with more accurate pyranometers at regularly maintained AWS locations (Eppley PSP measurements at Swiss Camp and

Table 3
GC-Net instruments used at the Greenland AWS relevant to this study and their accuracy

Location	Parameter	Instrument	Spectral sensitivity (μm)	Approximate uncertainty (%)	Sampling rate (s)
GC-Net Sites	Downwelling shortwave	LI-COR 200SZ	0.4–1.1	5	15
	Upwelling shortwave	LI-COR 200SZ	0.4–1.1	10	15
	Net radiation	REBS Q*7	0.35–30	20	15
Summit	Downwelling shortwave	Kipp and Zonen CM 21 Pyranometer	0.305–2.800	2	1
	Upwelling shortwave	Kipp and Zonen CM 21 Pyranometer	0.305–2.800	2	1
	Net radiation	Combination of the above four components		5	1
Swiss Camp	Downwelling shortwave	Eppley Pyranometer	0.2–3.5	7	1
	Upwelling shortwave	Eppley Pyranometer	0.2–3.5	7	1
	Downwelling longwave	Eppley Pyrageometer	4–50	15	15
Tunu-N	Downwelling shortwave	Eppley Pyranometer	0.2–3.5	7	1
	Upwelling shortwave	Eppley Pyranometer	0.2–3.5	7	1

TUNU-N; with Kipp and Zonen CM21 measurements from Summit; data courtesy of K. Steffen). For Swiss Camp comparisons, upward and downward shortwave irradiance errors did not exceed 2.7%. At Summit, downward shortwave errors were within 1.8%. A positive bias of 2.5% and 18.3% was observed in the reflected shortwave irradiance at Swiss Camp and TUNU-N, respectively. The corresponding albedo overestimation by the LI-COR pyranometer varied between 0.04 and 0.09 at the calibration sites (Table 3). At Swiss Camp, Summit, and TUNU-N, where precise comparative measurements were made, the average albedo for the GC-Net analysis is reduced globally by 0.04, 0.07, and 0.09, respectively. Upward shortwave irradiance values at all other GC-Net sites were reduced by offset values ranging from 0.01 to 0.09 to produce albedo values of 0.87 for clear-sky cases following fresh snow accumulation episodes. This procedure has been verified at the sites where precision pyranometer data were available. A more sophisticated correction procedure is not offered (e.g., to account for changes in grain size and water content) owing to the lack of information about these quantities. None of the downward solar irradiance values was adjusted in this study beyond their factory calibrations.

The systematic error in in situ observations has been corrected to first order and should no longer greatly contributes to the in situ uncertainty. Once this correction is made, the in situ uncertainty is dominated by random effects (i.e., persistent leveling error, cosine-response error, tower interference with the radiation environment, and microscale environmental noise). Comparisons with precision pyranometer measurements suggest the residual LI-COR 200SZ uncertainty has an RMSE of 0.035. Therefore, conclusions concerning any MODIS albedo errors exceeding 0.035 will have noteworthy statistical significance.

3.2. Cloud detection

Clear-sky albedos were determined from the hourly in situ data by comparing observed incoming solar irradiance with clear-sky irradiance calculations from the FluxNet radiative transfer model (Key & Schweiger, 1998). Effective cloud transmittance (T_e) was computed as a means of discerning clear-sky conditions. T_e is defined as the ratio of measured incoming solar radiation to that computed by a radiative transfer model (Box, 1997). A value of 1.0 implies clear-sky conditions. Although an increase in diffuse sky irradiance in the presence of thin clouds will cause underestimates of the true cloud amount, we aim only to discriminate between cloudy and clear conditions. The frequency distributions of T_e values suggest a threshold value of T_e>0.8 for discriminating between clear and cloudy conditions in the MODIS data. The presence of optically thin clouds can cause false selection of clear-sky cases. However, this type of error is believed to occur in only a minority of the samples.

Next, the daily mean albedo for each day is computed by weighting the hourly albedo (α_{hour}) measurements by the cosine of the solar zenith angle (μ). This is done for all the daily observations ("all-sky") and for "clear-sky"-only observations according to the following equation:

$$\text{Daily Mean Albedo} = \int_{\mu_{\min}}^{\mu_{\max}} \alpha_{\text{hour}}(\mu)\mu \mathrm{d}\mu$$

The solar zenith angle is limited to angles less than 75° in computing the daily mean albedo for both the all-sky and clear-sky albedos from the in situ data. Finally, the 16-day albedo is computed by averaging the daily mean albedo over the 16-day time periods corresponding to the MODIS 16-day product.

In making comparisons discussed in Section 4, only results using the center pixel from the 3×3 pixel area extracted from the MODIS data set are presented in order to minimize differences resulting from spatial variability, especially at the lower elevation sites that experience significant summer melt. While the in situ data represent point measurements of ~4 m^2, the MODIS values represent a 1-km^2 area centered over each site. Therefore, spatial scale differences in sampling introduce some amount of error in our comparison that cannot be attributed to either in situ or MODIS data. Without in situ albedo sampling at varying scales within the MODIS footprint (pixel), we cannot eliminate this source of error. While we acknowledge that, at certain locations, there could be intrinsic heterogeneity due to melt, wind structures, water pooling, dust concentrations, etc., we did not make an attempt to compensate for these factors in this initial validation of the MODIS 16-day albedo product. However, in most cases, this scale gap error is a second-order effect that we neglect in the present work, but would propose as part of future field work. Currently, the MODIS geolocation accuracy is better than 150 m at the 99% confidence interval (Wolfe et al., 2002).

4. Results

As a first assessment of the MODIS 16-day albedo product accuracy, we compare daily mean in situ clear-sky albedo with the MODIS 16-day albedo estimates. Fig. 2 shows a comparison at stations along an elevation transect from a zone of melting into the dry-snow zone during 2002. Results are shown for both the MODIS BSA and the WSA.

In the ablation zone, at the JAR3, JAR2, JAR1, and Swiss Camp sites, the in situ albedo variability is closely matched by the MODIS albedo variability. Negative bias of the MODIS 16-day albedo at JAR3 and JAR1 may be attributed to persistent microscale surface inhomogeneities (e.g., melt ponds, crevasses, etc.) in 2002, particularly during the active melt season. At JAR3, the negative bias in the MODIS albedo is likely a result of this station's proximity to land (~150–300 m from seasonally snow-free land). At JAR1, the negative bias of the MODIS albedo during summer may be a result of large melt lakes that form near this station, as well as other surface inhomogeneities. This would not, however, explain the bias observed early in the season. The same surface inhomogeneities are expected also at JAR2, but here the MODIS albedo matches up quite well with the in situ albedo during 2002 except for two outliers.

The surface is more homogeneous in the higher elevation zone (e.g., ~2000 m and above) of little or no melting, and provides a less ambiguous comparison between a 1-km satellite product and a ground-based point measurement. At Crawford Point 1, near 2000 m elevation, and Summit (3150 m), the MODIS albedo also agrees in general quite well with the measurements in 2002, although some large differences are observed occasionally at the Summit station.

Scatterplots between the MODIS and in situ 16-day mean albedo for the individual stations using all available data from 2000 to 2003 are presented in Fig. 3a–p. Results are shown for all stations listed in Table 2 except for stations 4, 11, 18, and 20. At these stations, there were either not enough "high-quality" MODIS or in situ data to make a comparison with. Scatterplots combining all the stations are shown in Fig. 4a and b. In the figures, results are shown for the clear-sky in situ albedo versus both the clear-sky MODIS WSA and BSA. A distinction is made between retrievals using the primary model, "main" (solid symbols), and the secondary backup algorithm, "backup" (open symbols). It is important to remember that even though a retrieval is obtained from the backup algorithm, as mentioned in Section 2.2, the backup algorithm may perform quite well and the albedo may actually match the in situ measurement. An example of this might occur if only a few angular samples are available but they represent accurate observations with very little noise and an appropriate underlying BRDF shape is available.

At stations where there is a large seasonal variation in albedo (i.e., sites in the seasonal melt zone; e.g., JAR1, JAR2, JAR3, Swiss Camp), the correlation coefficient between the MODIS BSA and in situ data is high (above 0.8) (Table 4). The same is true for the MODIS WSA albedo, the only exception at Swiss Camp where the correlation between the WSA and in situ albedo drops below 0.8. At JAR3, mixed pixels may affect the comparison since the station is less than 200 m from ice-free land. At low elevations, summer melting commonly exceeds 2 m, and results in the accumulation of dust (cryoconite) on the surface. Local albedo variability is expected depending on whether the AWS is over different kinds of patches (e.g., snow, ice, puddles, clean ice, dusty ice, etc.). This variability will contribute to disagreements between the satellite and station measurements in the ablation region of the ice sheet. At JAR2, there is a general positive bias in the MODIS albedo. It could be that local melting under the AWS tower during certain years is responsible for the in situ data generally being lower than the MODIS albedo at this site. Another cause could be that the in situ sensor was looking at bare ice, while the MODIS pixel contains a mixture of snow/ice types.

Table 4 lists the correlation coefficient derived from least squares regression between the MODIS and AWS albedo, as well as the significance of the regression (F test and P values), mean differences, standard deviation, and RMSE. Mean differences between the MODIS main algorithm retrievals and the in situ data are also shown in Table 4. In the table, we include results for both the clear-sky and all-sky in situ albedos in order to illustrate how sensitive the results are to the use of the 0.8 T_e threshold in defining clear-sky conditions from the in situ data. Stations with high correlation coefficients (e.g., a strong relationship between the MODIS and in situ albedo) also have higher statistically significant relationships (high F test value and low P value) than those with weak correlations. Sites with little seasonal variation in albedo show very low correlation between MODIS and in situ albedo because of the small range in albedo values (standard deviation of in situ albedo of less than 0.02). At these sites, however, the relative error is still within an acceptable range (typically less than 0.08 RMSE), given the anticipated errors in the in situ data (0.035 RMSE).

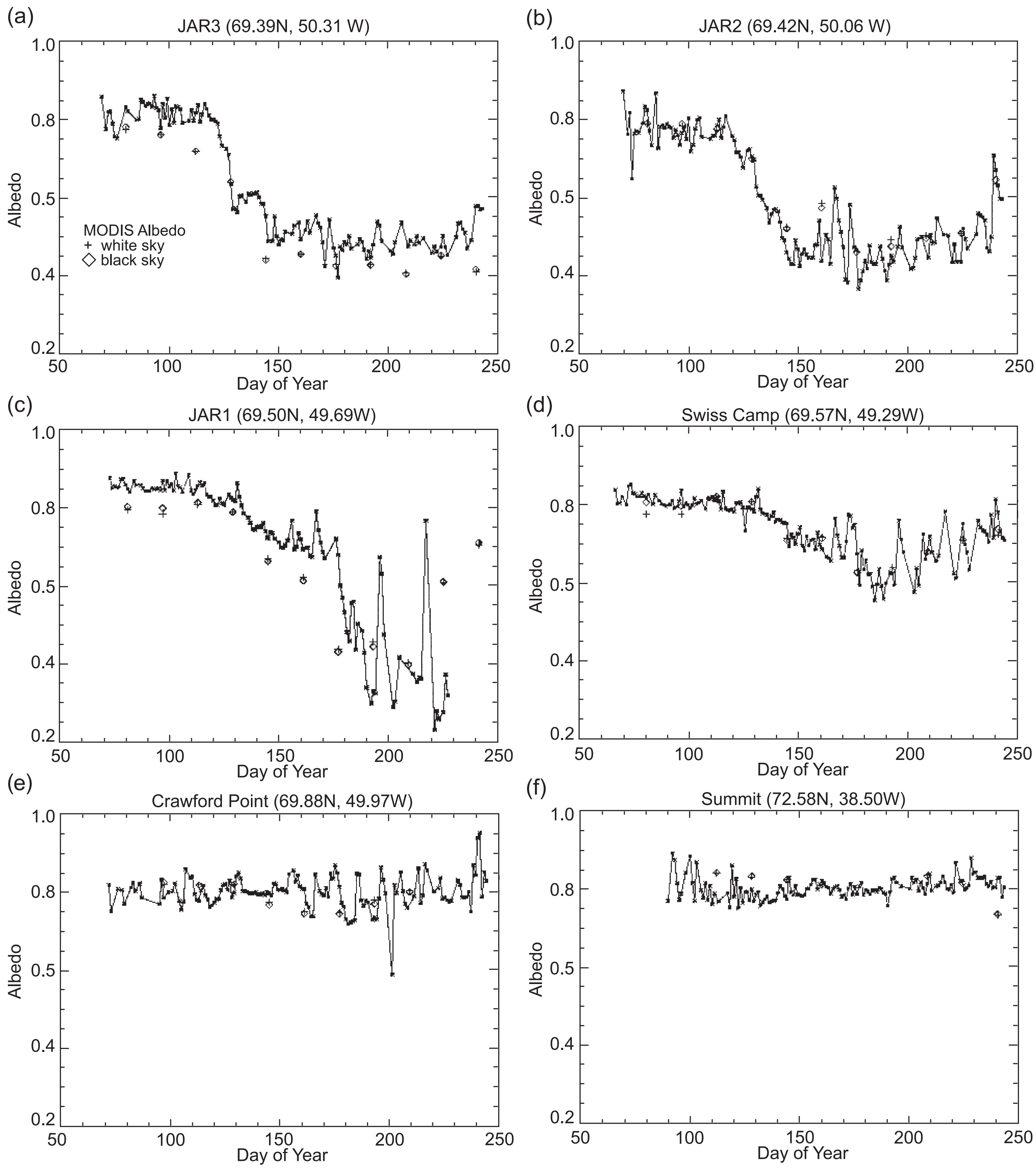

Fig. 2. Daily-averaged, clear-sky in situ albedo data at JAR3 (a), JAR2 (b), JAR1 (c), Swiss Camp (d), Crawford Point (e), and Summit (f) during 2002. The MOD43 16-day albedos are also shown for both the WSA (+) and BSA (triangles).

The best agreement between the two albedo data sets was found at JAR1 (Fig. 3h). There is, however, a positive MODIS albedo bias during periods when the sun is low in the sky because the backup algorithm tends to be used more frequently for such cases. However, not all the backup algorithm retrievals occur during periods of large solar zenith angle, nor do they always result in a positive bias. But the fact that many of the backup algorithm retrievals do occur when the solar zenith angle is large (at this and other stations) indicates that relatively large MODIS BRDF retrieval errors (errors as large as 0.2 in absolute albedo) may occur at high solar zenith angles. The solar zenith angle of the midpoint of each 16-day period is listed in Table 5 as a function of the MODIS 16-day production period. Besides affecting the accuracy of the BRDF algorithm, the accuracy of the atmospheric correction algorithm also degrades as the solar zenith increases. We limited the in situ data to cases where the solar zenith angle is less than 75°, and the

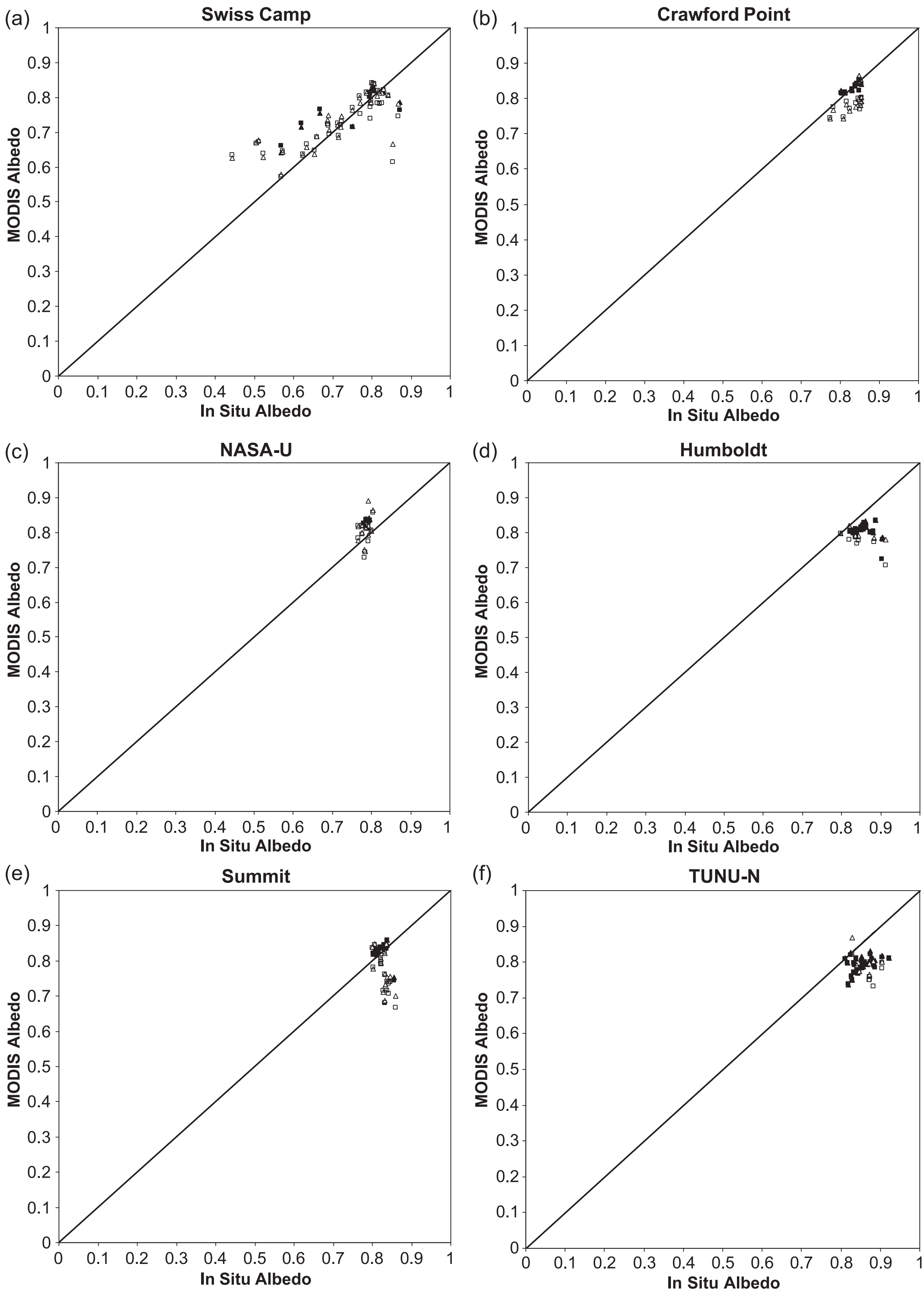

Fig. 3. Comparison between clear-sky MOD43 16-day albedo and 16-day in situ albedo for both the BSA (triangles) and WSA (squares). A distinction is made between MOD43 retrievals using the "main" algorithm (closed symbols) and the "backup" algorithm (open symbols). The solid line represents the 1:1 line or zero error line.

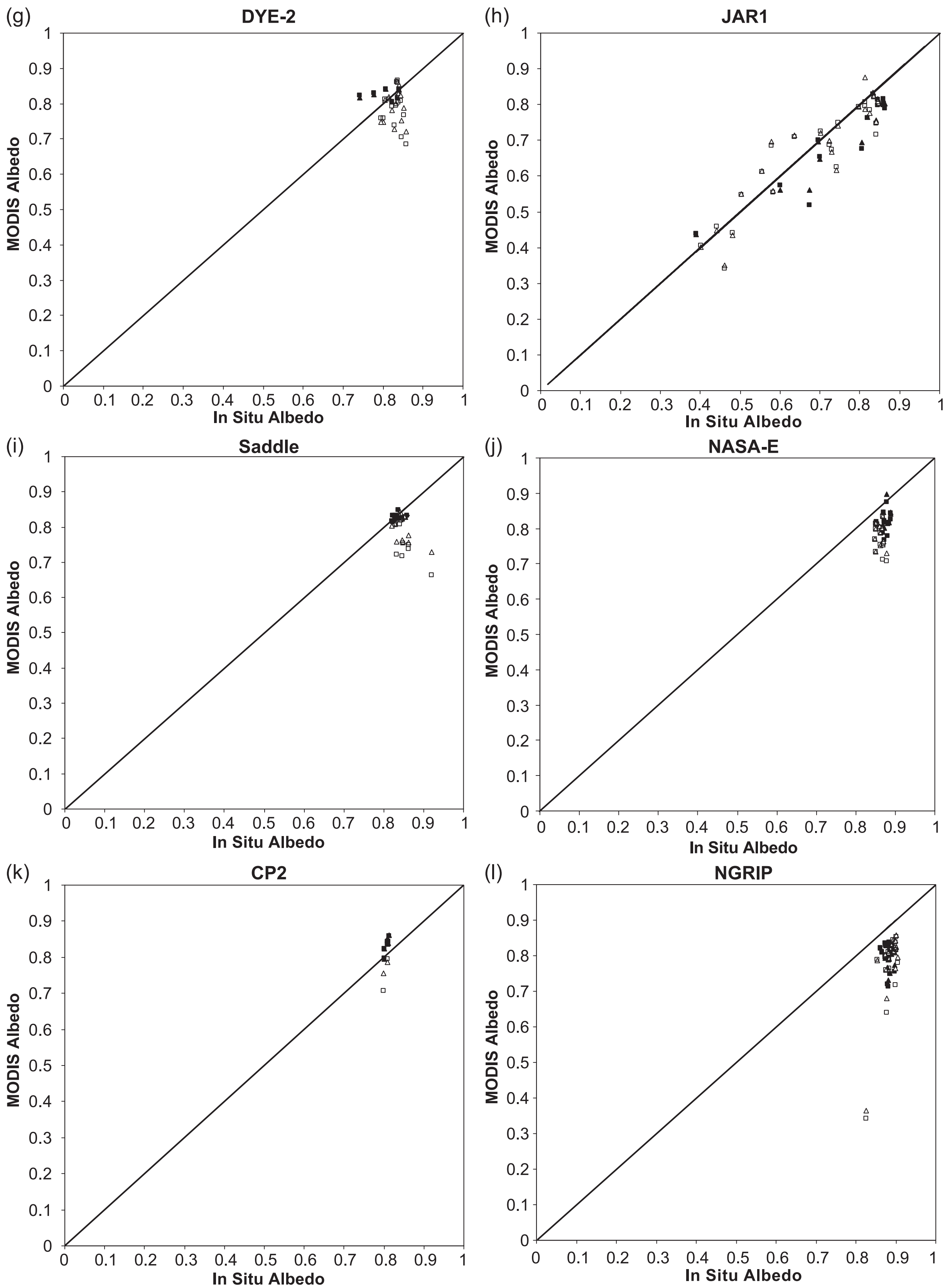

Fig. 3 (*continued*).

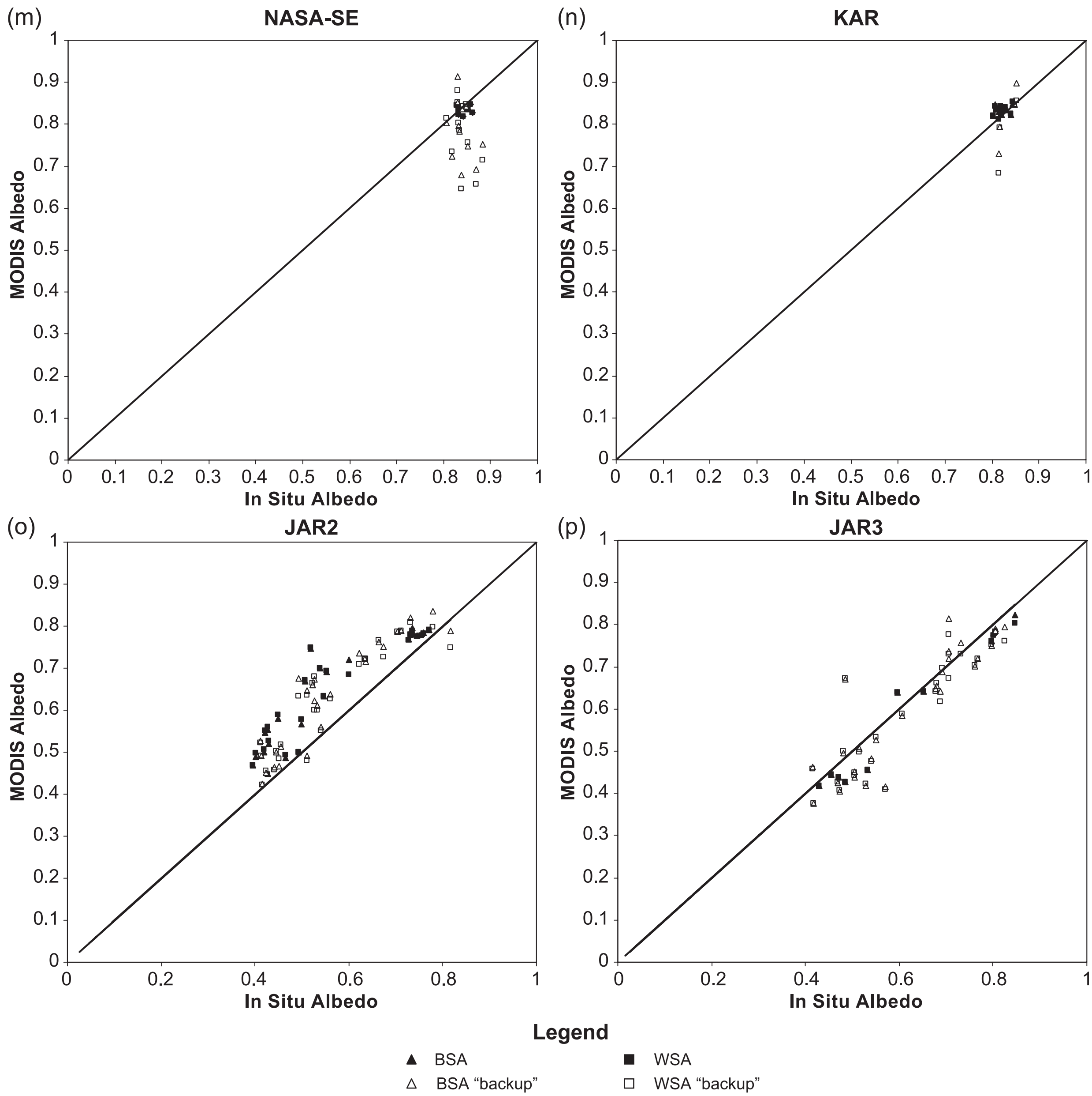

Fig. 3 (*continued*).

contributions of the surface reflectance inputs to the MODIS albedo algorithm, while not explicitly constrained to solar zenith angles of less than 75°, are constrained by their quality flags. Lower-quality inputs (i.e., solar zenith angle >75°) will get lower weights according to the MODIS BRDF/albedo algorithm. Thus, the final retrieval qualities that are saved as a part of the standard MODIS BRDF/albedo products also reflect the quality of the input data.

At Swiss Camp (Fig. 3a), we expected that large glacial melt lakes forming in the vicinity (within 1 km) of the AWS would result in low summer MODIS albedo biases (e.g., larger scatter among low albedo values). The albedo of the lakes depends on their depth and can drop to values below 0.2 for depths exceeding 1 m. However, such decreases in MODIS albedo are not observed in Fig. 3a. We hypothesize that the high MODIS albedo biases may result from local melting under the AWS tower, which is not observed at the spatial scale of the MODIS instrument. This could explain why, in 2003, the MODIS-retrieved surface albedo during midsummer is systematically higher than the in situ measurements. The large scatter around high albedo values at Swiss Camp primarily occurs at times when solar zenith angles are large (and are flagged as lower-quality retrievals since the backup algorithm is used).

At higher elevation sites, a systematic positive bias of about 0.07 in the MODIS albedo is observed for most of the northern stations (i.e., Humboldt, TUNU-N, NASA-E, and NGRIP) for both the backup and main algorithm retrievals,

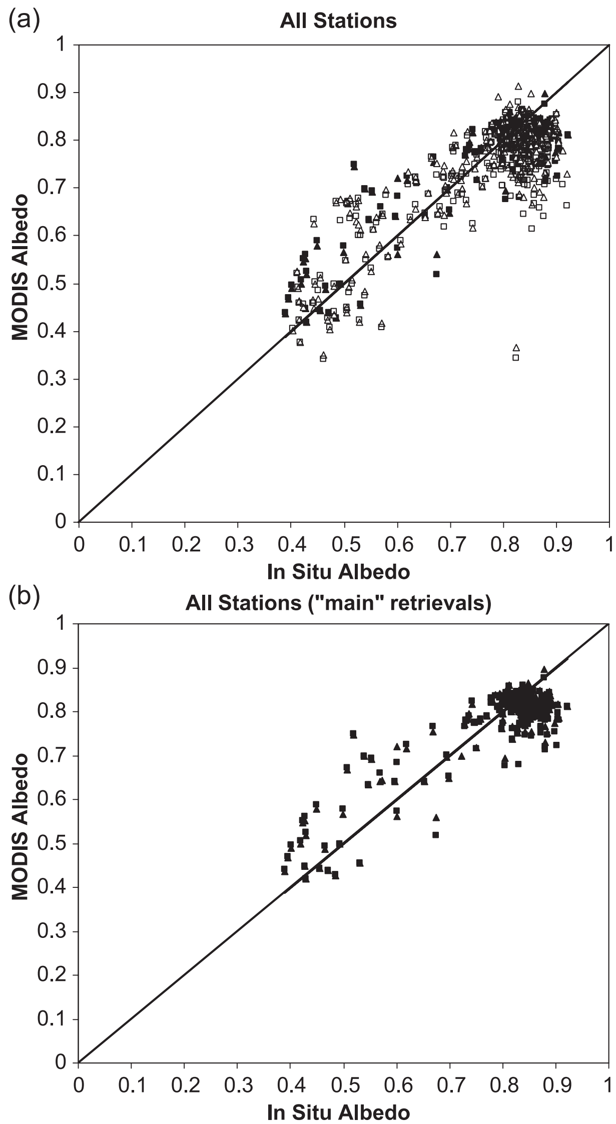

Fig. 4. (a) Comparison between clear-sky MOD43 16-day albedo and 16-day in situ albedo for both the BSA and WSA combined for all the stations examined in Fig. 3a–o. The solid line represents the 1:1 line or zero error line. MODIS albedos from both the "main" and "backup" algorithm results are shown. (b) Comparison between clear-sky MOD43 16-day albedo and 16-day in situ albedo for both the BSA and WSA combined for all the stations examined in Fig. 3a–p. The solid line represents the 1:1 line or zero error line. MODIS albedos from only the "main" algorithm results are shown.

although this bias decreases substantially at some of these sites if we only consider the main retrievals (Table 4). At TUNU-N, we believe part of the bias is a result of errors in the in situ data since the albedo is observed to drift to values greater than 0.9. The mean MODIS BSA albedo (combined backup and main algorithm retrievals) for TUNU-N is 0.79 versus 0.86 for the in situ data. Likewise at NGRIP, the mean in situ albedo is 0.88 versus 0.79 for the MODIS BSA albedo. However, the mean value for main retrievals is 0.82 while that for the backup algorithm retrievals is 0.77. In general, the broadband albedo value of fresh dry snow is known to be about 0.84 (Konzelman & Ohmura, 1995). In summer months, we would expect this value to drop slightly, so it appears that there may still be a slight positive bias in the GC-Net albedo at these sites. Another important factor to consider is that the GC-Net albedo values increase with increasing solar zenith angle. This alone implies that higher mean albedo values are to be expected for the northern stations, despite the dry-snow conditions.

At Humboldt (Fig. 3d), the mean difference between the albedo reported in Table 4 is dominated by discrepancies observed in 2000 and 2003 when the sun was low in the sky (e.g., during spring in 2000 and during autumn in 2003). There appears to be a drift in the in situ albedo during these two time periods, which causes the in situ albedo to exceed 0.9 and must be an observational data error, likely a result of leveling errors. Otherwise, the mean difference in the albedo would be more on the order of 0.04.

At NASA-E (Fig. 3j), the in situ albedo is relatively constant, whereas the MODIS albedo shows large oscillations (albedo varies from 0.7 to 0.9). This appears to be caused primarily by the backup algorithm retrievals. The standard deviation for backup algorithm retrievals is 0.044, which is twice as large for main algorithm retrievals (0.022).

Saddle (Fig. 3i) and NASA-SE (Fig. 3l) are located within 104 km of each other and show similar results. At Saddle, the MODIS and in situ albedo are within 0.03 of each other, on average. If the five data points that are labeled as "backup" are removed, the mean albedo difference is essentially 0. The same is true for NASA-SE after removing the identical five data points in the analysis, although at this station the agreement between the MODIS and in situ albedo is not as strong or as significant as it is at Saddle. Therefore, one may conclude that for the cases examined here, the backup algorithm is not as robust as the main one.

Although both Crawford Points 1 and 2 (stations 2 and 13, respectively) are located in the accumulation region of the ice sheet, melt has been observed in recent years at these stations, especially in 2002 and 2003. The MODIS albedo product captures this larger seasonal variability, and this larger albedo variability is also reflected in the higher correlation coefficients for these sites.

In general, the MODIS albedo data at the Summit station (Fig. 3e) match the in situ albedos quite well (mean differences for main algorithm all less than or equal to 0.012) if we consider only the main algorithm retrievals. Most of the backup algorithm retrievals significantly underestimate the measured albedo, and these mostly occur under conditions of high solar zenith angle. However, during the year 2000, from day 177 onwards, all the MODIS albedos are labeled as "backup," emphasizing again that it is not possible to say that all the backup algorithm retrievals occur under conditions of high solar zenith angles. Other factors contribute to the poor-quality flags during the latter half of 2000, such as an insufficient number of angular samples of the available surface reflectance.

Table 4
Statistical summary of differences between MODIS and in situ albedo

Station	Correlation coefficient	*F* test	*P* value	RMSE	Mean difference	S.D.	Mean difference for main algorithm retrievals
(1) Swiss Camp							
All-sky/BSA	0.829	94.550	0.0000	0.064	−0.020	0.064	−0.021
All-sky/WSA	0.751	55.502	0.0000	0.075	−0.013	0.073	−0.020
Clear-sky/BSA	0.825	91.326	0.0000	0.064	−0.012	0.061	0.016
Clear-sky/WSA	0.727	48.086	0.0000	0.074	−0.005	0.073	0.045
(2) Crawford Point							
All-sky/BSA	0.555	10.677	0.0033	0.036	0.020	0.029	0.002
All-sky/WSA	0.516	8.7270	0.0069	0.035	0.021	0.028	0.004
Clear-sky/BSA	0.564	11.185	0.0027	0.032	0.012	0.029	−0.004
Clear-sky/WSA	0.545	10.145	0.0040	0.031	0.013	0.027	−0.002
(3) NASA-U							
All-sky/BSA	0.404	3.1231	0.0963	0.046	−0.030	0.032	0.079
All-sky/WSA	0.318	1.7949	0.1991	0.040	−0.023	0.031	−0.039
Clear-sky/BSA	0.490	5.0481	0.0391	0.044	−0.028	0.031	−0.037
Clear-sky/WSA	0.443	3.8998	0.0658	0.038	−0.021	0.029	−0.034
(4) Humboldt							
All-sky/BSA	0.073	0.13367	0.7177	0.057	0.046	0.031	0.046
All-sky/WSA	0.379	4.1875	0.0514	0.073	0.055	0.045	0.051
Clear-sky/BSA	0.027	0.01737	0.8962	0.056	0.044	0.031	0.046
Clear-sky/WSA	0.369	3.9551	0.0578	0.073	0.054	0.046	0.051
(5) Summit							
All-sky/BSA	0.503	10.142	0.0034	0.065	0.027	0.058	−0.007
All-sky/WSA	0.565	14.054	0.0008	0.074	0.032	0.065	0.003
Clear-sky/BSA	0.368	4.7051	0.0381	0.061	0.020	0.056	−0.012
Clear-sky/WSA	0.401	5.7544	0.0029	0.069	0.025	0.063	−0.012
(6) TUNU-N							
All-sky/BSA	0.269	2.9536	0.0938	0.071	0.063	0.031	0.061
All-sky/WSA	0.104	0.4194	0.5211	0.079	0.070	0.033	0.063
Clear-sky/BSA	0.249	2.5067	0.1217	0.074	0.065	0.033	0.062
Clear-sky/WSA	0.039	0.0579	0.8111	0.083	0.072	0.036	0.065
(7) DYE-2							
All-sky/BSA	0.030	0.01859	0.8929	0.055	0.018	0.050	−0.020
All-sky/WSA	0.218	1.0000	0.3291	0.065	0.024	0.059	−0.010
Clear-sky/BSA	0.033	0.02154	0.8848	0.055	0.017	0.051	−0.019
Clear-sky/WSA	0.155	0.49309	0.4906	0.065	0.022	0.059	−0.020
(8) JAR1							
All-sky/BSA	0.927	206.32	0.0000	0.062	0.025	0.056	0.044
All-sky/WSA	0.919	286.36	0.0000	0.058	0.029	0.058	0.050
Clear-sky/BSA	0.922	193.25	0.0000	0.059	0.015	0.056	0.037
Clear-sky/WSA	0.911	166.12	0.0000	0.064	0.020	0.060	0.043
(9) Saddle							
All-sky/BSA	0.532	9.0774	0.0062	0.059	0.034	0.046	0.008
All-sky/WSA	0.635	15.518	0.0007	0.077	0.043	0.061	0.008
Clear-sky/BSA	0.580	11.684	0.0024	0.057	0.029	0.049	0.000
Clear-sky/WSA	0.663	18.007	0.0003	0.075	0.037	0.064	0.000
(10) NASA-E							
All-sky/BSA	0.393	4.1881	0.0523	0.075	0.064	0.035	0.049
All-sky/WSA	0.233	1.3227	0.2619	0.085	0.071	0.040	0.058
Clear-sky/BSA	0.440	5.5255	0.0277	0.073	0.062	0.034	0.048
Clear-sky/WSA	0.276	1.9057	0.1807	0.082	0.069	0.039	0.057

(*continued on next page*)

Table 4 (*continued*)

Station	Correlation coefficient	*F* test	*P* value	RMSE	Mean difference	S.D.	Mean difference for main algorithm retrievals
(11) CP2							
All-sky/BSA	0.765	8.4848	0.0269	0.038	−0.012	0.032	−0.027
All-sky/WSA	0.757	8.0537	0.0296	0.049	−0.007	0.045	−0.026
Clear-sky/BSA	0.760	8.1844	0.0288	0.038	−0.016	0.030	−0.030
Clear-sky/WSA	0.704	5.8831	0.0515	0.048	−0.010	0.043	−0.029
(12) NGRIP							
All-sky/BSA	0.649	26.275	0.0000	0.113	0.087	0.068	0.074
All-sky/WSA	0.598	20.053	0.0001	0.122	0.093	0.074	0.081
Clear-sky/BSA	0.035	0.04275	0.8374	0.120	0.088	0.079	0.069
Clear-sky/WSA	0.053	0.10027	0.7533	0.129	0.094	0.084	0.076
(13) NASA-SE							
All-sky/BSA	0.232	1.0212	0.3256	0.077	0.036	0.065	0.009
All-sky/WSA	0.331	2.2189	0.1536	0.086	0.041	0.073	0.009
Clear-sky/BSA	0.343	2.3978	0.1389	0.082	0.033	0.073	0.003
Clear-sky/WSA	0.453	4.6556	0.0447	0.092	0.037	0.082	0.003
(14) KAR							
All-sky/BSA	0.492	4.1600	0.0623	0.032	−0.005	0.031	−0.012
All-sky/WSA	0.380	2.1906	0.1627	0.040	0.002	0.039	−0.011
Clear-sky/BSA	0.400	2.4809	0.1392	0.040	−0.020	0.033	−0.031
Clear-sky/WSA	0.211	0.6089	0.4492	0.046	−0.013	0.043	−0.030
(15) JAR2							
All-sky/BSA	0.914	255.19	0.0000	0.094	−0.077	0.052	−0.081
All-sky/WSA	0.901	228.54	0.0000	0.092	−0.073	0.054	−0.082
Clear-sky/BSA	0.867	151.98	0.0000	0.091	−0.061	0.067	−0.072
Clear-sky/WSA	0.852	132.80	0.0000	0.091	−0.057	0.070	−0.044
(16) JAR3							
All-sky/BSA	0.917	168.76	0.0000	0.063	0.022	0.058	0.024
All-sky/WSA	0.919	173.33	0.0000	0.062	0.025	0.056	0.026
Clear-sky/BSA	0.878	107.40	0.0000	0.076	0.027	0.070	0.037
Clear-sky/WSA	0.873	102.53	0.0000	0.077	0.031	0.069	0.038
(17) All stations							
All-sky/BSA	0.861	1294.7	0.0000	0.069	0.018	0.067	0.011
All-sky/WSA	0.841	1083.3	0.0000	0.075	0.024	0.071	0.015
Clear-sky/BSA	0.848	1150.1	0.0000	0.070	0.019	0.068	0.012
Clear-sky/WSA	0.823	942.01	0.0000	0.077	0.024	0.073	0.016

Note that in producing this table, all MODIS retrievals were used, including the "poor"-labeled observations for the statistics. The last column gives the mean difference for the "main" algorithm retrievals. Mean difference is the in situ albedo minus the MODIS albedo.

At DYE-2 (Fig. 3g), agreement between MODIS and in situ data is poor. The MODIS albedo exhibits large oscillations on the order of 0.10 (e.g., similar to what is seen in Fig. 2f) that are not observed in the station data. However, many of the MODIS retrievals are labeled as "backup" at this station, and thus it is difficult to clearly assess the accuracy at this station. Disagreement between the MODIS albedos and in situ measurements may, in part, be a result of the presence of a large radar station and runway near the AWS tower at DYE-2. Lastly, at KAR (Fig. 3m), the agreement is very good between the satellite and station measurement, with mean differences in albedo of around 0.02 (~0.01 after removing the backup algorithm retrievals found at low sun angles).

Fig. 4 summarizes the results for all the Greenland sites. The mean difference between the MODIS clear-sky BSA

Table 5
The medium solar zenith angle of the 16-day period for 75° north

Period (Julian day)	049	065	081	097	113	129	145	161	177	193	209	225	241	257	273
Medium size at passing time (°)	87.9	81.8	75.5	69.3	63.8	59.5	56.5	55.1	55.5	57.6	61.2	66.1	71.9	78.3	84.5

and in situ albedo is 0.02, and the RMSE is 0.07. If we consider only the main algorithm retrievals, then the RMSE drops to 0.04 and the mean differences are all less than 0.02.

The above results focused on comparing both the MODIS black-sky and white-sky albedo to ground-based snow albedo measurements. However, the actual albedo is a combination of the BSA and WSA albedo, and will depend on the particular atmospheric conditions under which the observation was made. At most solar zenith angles, the BSA and WSA bracket the actual albedo. Since in situ measurements of atmospheric optical depth were not available, we did not compute the actual albedo from the MODIS data. Note, however, that, in general, the BSA and WSA at these local solar noon zenith angles are nearly identical (they are identical at approximately 50°) and therefore close to the actual albedo, as would be measured at the surface. Thus, the statistical results shown in Table 4 are often similar for the BSA and WSA retrievals. Exceptions occur primarily during spring and autumn when the solar zenith angle often exceeds 50°, but at those times, the quality of the MODIS albedos is often flagged as poor (e.g., the backup algorithm is used). Therefore, the statistical differences between the BSA and WSA have more to do with backup versus main algorithm retrievals than with BSA versus WSA.

5. Conclusions

This study has shown that high-quality MODIS albedo retrievals, albeit limited in extent, can be obtained over homogeneous snow surfaces. The mean difference between the MODIS algorithm retrievals and the in situ data is less than 0.02 for all the stations combined (RMSE=0.07). This result is based on all the MODIS albedo retrievals that include use of both the main and backup algorithms. Using only the main algorithm retrievals, the RMSE drops to 0.04 and the mean differences in albedo are less than 0.02 at all sites. While the magnitude of individual in situ albedo uncertainties is nearly that of the result for individual MODIS 16-day product results, uncertainties concerning MODIS albedo variability across the entire range of observations (i.e., 0.39–0.88) are well within the trends observed in the ground data. Moreover, we can conclude that the MODIS albedo product is reliable in observing variability below albedo values of 0.07, which are of primary importance to ice sheet mass balance studies.

The quality of the MODIS albedo product will continue to improve with continued improvements in atmospheric correction and cloud detection in the MODIS processing stream. We are not aware of any publications on the improvements in accuracies between V003 and V004 MOD43 albedo products, although accuracies are stated on the MODIS Land Team (MODLAND) validation web site (http://landval.gsfc.nasa.gov/MODIS/index.php). However, since the MODIS results presented here agree, in general, with the observations (within ±0.07), it is likely that the MODIS albedo algorithm is reliable in selecting only the clear-sky observations. Furthermore, even though the MODIS atmospheric correction over Greenland does not presently include the influence of aerosols, the conservative nature of the MODIS albedo algorithm in accepting only high-quality inputs, coupled with the small amount of aerosols typically found over Greenland on cloud-free days and the relative impact of residual aerosols on the surface reflectance of such a bright surface, indicates that aerosol contamination only minimally impacts the multiday retrieval.

Obviously, more frequent retrievals would better capture changes in snow conditions (i.e., melt variability). The 16-day time step of the MODIS algorithm is somewhat problematic for snow surfaces, which can change rapidly due to melting, rain-on-snow, wind sculpting of the surface, and development of surface hoar frost. A possible alternative approach that would capture shorter-term albedo variations is a daily BRDF retrieval algorithm that uses a 16-day sliding window and a weighting scheme to emphasize the most recent observations.

The quality flags describe the quality of input samples in terms of atmospheric correction, number of observations, and angular distribution of samples, and indicate whether the main or backup algorithms were used in the retrieval. Although our validation results show that the inversions from the backup algorithm can produce reliable data in some cases, they confirm that, in general, the backup algorithm albedo retrievals with low-quality flags have lower accuracies than albedos from full inversions (“good quality”). Based on the limited number of validation sites studied thus far (Jin et al., 2003a,b; Liang et al., 2002; Wang et al., 2004), the MODIS BRDF/albedo product has been assigned a Validated Stage 1 accuracy with full inversions falling within 5%, with the majority of the backup magnitude inversions falling within 8–11%. The results of this study over spatially homogeneous snow concur with this accuracy.

Finally, accurately measuring albedo at high latitudes is challenging, not only for ground measurements, but also from satellite. Reflectance measurements made at high solar zenith angles pose difficulties in calibration and atmospheric correction. As shown in Table 5, about half of available satellite observations during the sunlit season are obtained under conditions where the solar zenith angle exceeds 70°. While more studies need to be conducted on how these high solar zenith angle observations affect the BRDF retrievals, at present, these lower-quality results (that occur because of high solar zenith angles) should be avoided.

References

Bicheron, P., & Leroy, M. (2000). Bidirectional reflectance distribution function signatures of major biomes observed from space. *Journal of Geophysical Research*, *105*, 26,669–26,681.

Box, J. (1997). *Polar day effective cloud opacity in the Arctic from measured and modeled solar radiation fluxes*, MA Thesis, University of Colorado, Boulder, CO.

Friedl, M. A., McIver, D. K., Hodges, J. C. F., Zhang, X. Y., Muchoney, D., Strahler, A. H., et al. (2002). Global land cover mapping from MODIS: Algorithms and early results. *Remote Sensing of Environment*, *83*, 287–302.

Jin, Y., Schaaf, C. B., Gao, F., Li, X., Strahler, A. H., Lucht, W., et al. (2003a). Consistency of MODIS surface bidirectional reflectance distribution function and albedo retrievals: 1. Algorithm performance. *Journal of Geophysical Research*, *108*(D5).

Jin, Y., Schaaf, C. B., Woodcock, C. E., Gao, F., Li, X., Strahler, A. H., et al. (2003b). Consistency of MODIS surface bidirectional reflectance distribution function and albedo retrievals: 2. Validation. *Journal of Geophysical Research*, *108*(D5).

Key, J., & Schweiger, A. J. (1998). Tools for atmospheric radiative transfer: Streamer and FluxNet. *Computers and Geosciences*, *24*(5), 443–451.

Klein, A. G., & Stroeve, J. (2002). Development and validation of a snow albedo algorithm for the MODIS instrument. *Annals of Glaciology*, *34*, 45–52.

Konzelmann, T., & Ohmura, A. (1995). Radiative fluxes and their impact on the energy balance of the Greenland ice sheet. *Journal of Glaciology*, *41*(139), 490–502.

Leroy, M., & Hautecoeur, O. (1999). Anisotropy-corrected vegetation indexes derived from POLDER/ADEOS. *IEEE Transactions on Geoscience and Remote Sensing*, *37*, 1698–1708.

Li, X., & Strahler, A. H. (1992). Geometric–optical bidirectional reflectance modeling of the discrete crown vegetation canopy: Effect of crown shape and mutual shadowing. *IEEE Transactions on Geoscience and Remote Sensing*, *30*, 276–292.

Liang, S., Fang, H., Chen, M., Shuey, C. J., Walthall, C., Daughtry, C., et al. (2002). Validating MODIS land surface reflectance and albedo products: Methods and preliminary results. *Remote Sensing of Environment*, *83*, 149–162.

Liang, S., Strahler, A. H., & Walthall, C. W. (1999). Retrieval of land surface albedo from satellite observations: A simulation study. *Journal of Applied Meteorology*, *38*, 712–725.

Lucht, W., & Lewis, P. (2000). Theoretical noise sensitivity of BRDF and albedo retrieval from the EOS-MODIS and MISR sensors with respect to angular sampling. *International Journal of Remote Sensing*, *21*, 81–98.

Lucht, W., Schaaf, C. B., & Strahler, A. H. (2000). An algorithm for the retrieval of albedo from space using semiempirical BRDF models. *IEEE Transactions on Geoscience and Remote Sensing*, 38,977–38,998.

Martonchik, J. V., Bruegge, C. J., & Strahler, A. H. (2001). A review of reflectance nomenclature used in Remote Sensing. *Remote Sensing Reviews*, *19*, 9–20.

Maslanik, J., Fowler, C., Key, J., Scambos, T., Hutchinson, T., & Emery, W. (1998). AVHRR-based Polar Pathfinder products for modeling applications. *Annals of Glaciology*, *25*, 388–392.

Privette, J. L., Eck, T. F., & Deering, D. W. (1997). Estimating spectral albedo and nadir reflectance through inversion of simple BRDF models with AVHRR/MODIS-like data. *Journal of Geophysical Research*, *102*, 29,529–29,542.

Ross, J. K. (1981). *The radiation regime and architecture of plant stands*. Norwell, MA: Dr. W. Junk, 392 pp.

Rossow, W. B., & Garder, L. (1984). Selection of a map grid for data-analysis and archival. *Journal of Climate and Applied Meteorology*, *23*(8), 1253–1257.

Roujean, J. L., Leroy, M., & Deschamps, P. Y. (1992). A bidirectional reflectance model of the Earth's surface for the correction of remote sensing data. *Journal of Geophysical Research*, *97*, 20,450–20,468.

Schaaf, C. B., Gao, F., Strahler, A. H., Lucht, W., Li, X., Tsang, T., et al. (2002). First operational BRDF, albedo and nadir reflectance products from MODIS. *Remote Sensing of Environment*, *83*, 135–148.

Snyder, J. P. (1987). *Map projections—a working manual*. U.S. Geological Survey Professional Paper 1395, Washington, DC, United States Government Printing Office.

Steffen, K., & Box, J. E. (2001). Surface climatology of the Greenland ice sheet: Greenland Climate Network 1995–1999. *Journal of Geophysical Research*, *106*(D24), 33951–33964.

Strugnell, N. C., & Lucht, W. (2001). An algorithm to infer continental-scale albedo from AVHRR data, land cover class, and field observations of typical BRDFs. *Journal of Climate*, *14*, 1360–1376.

Van Leeuwen, W., & Roujean, J. -L. (2002). Land surface albedo from the synergistic use of polar (EPS) and geo-stationary (MSG) observing systems: An assessment of physical uncertainties. *Remote Sensing of Environment*, *81*, 1–17.

Wang, K., Liu, J., Zhou, X., Sparrow, M., Ma, M., Sun, Z., et al. (2004). Validation of the MODIS global land surface product using ground measurements in a semi desert region on the Tibetan Plateau. *Journal of Geophysical Research*, *109*.

Wolfe, R., Nishihama, M., Fleig, A. J., Kuyper, J. A., Roy, D. P., Storey, J. C., & Patt, F. S. (2002). Achieving sub-pixel geolocation accuracy in support of MODIS land science. *Remote Sensing Environment*, *83*, 31–49.